# JUNO'S EARTH FLYBY: THE JOVIAN INFRARED AURORAL MAPPER PRELIMINARY RESULTS

A. Adriani[1], M.L. Moriconi[2], A. Mura[1], F. Tosi[1], G. Sindoni[1], R. Noschese[1], A. Cicchetti[1], G. Filacchione[1]

[1]*Institute for Space Astrophysics and Planetology, IAPS-INAF, Via Fosso del Cavaliere 100, Rome , Italy*

[2]*Institute of Climate and Atmospheric Science, ISAC-CNR, Via Fosso del Cavaliere 100, Rome, Italy*

## Abstract

The Jovian InfraRed Auroral Mapper, JIRAM, is an image-spectrometer onboard the NASA Juno spacecraft flying to Jupiter. The instrument has been designed to study the aurora and the atmosphere of the planet in the spectral range 2-5 μm. The very first scientific observation taken with the instrument was at the Moon just before Juno's Earth fly-by occurred on October 9, 2013. The purpose was to check the instrument regular operation modes and to optimize the instrumental performances. The testing activity will be completed with pointing and a spectral calibrations shortly after Jupiter Orbit Insertion. Then the reconstruction of some Moon infrared images, together with co-located spectra used to retrieve the lunar surface temperature, is a fundamental step in the instrument operation tuning. The main scope of this article is to serve as a reference to future users of the JIRAM datasets after public release with the NASA Planetary Data System.

**Keywords**: Jupiter, Moon, Instruments and techniques, Image processing, modeling

## 1. Introduction

[1]. The Juno mission is the second spacecraft designed under NASA's New Frontiers Program. The Juno spacecraft was launched in August 2011 with the primary goal to understand the origin and the evolution of Jupiter. The Juno payload includes an extensive suite of science instruments selected to satisfy the science objectives (Bolton, 2012). Among those instruments the Jupiter InfraRed Auroral Mapper (JIRAM) (Adriani et al., 2014) has the goal to sound Jupiter's aurora and, more in general, the upper layers of Jupiter's atmosphere. JIRAM benefits from the significant heritage coming from previous Italian-made visible and near infrared imaging spectrometers onboard Cassini, Rosetta, Venus Express and Dawn (Brown et al. 2004; Coradini et al. 2007; Piccioni et al. 2007; De Sanctis et al. 2011). In this paper we present the results of the Moon observations taken by JIRAM during Juno's Earth-Moon fly-by in October 2013.

[2]. JIRAM is a spectro-imager designed to investigate the Jovian aurora, retrieve the concentration of atmospheric gases in hot spots and constrain Jupiter's formation environment through the study of the composition and the abundances of chemical species in the Jovian atmosphere. Beyond the scientific value of the observation, this has been so far the first and unique occasion during the cruise phase to verify the execution of the science observing sequences as they will be operated at Jupiter. Here, the first elaboration of that series of observations is presented. The imager has been able to capture the Moon region straddling the terminator in L and M astronomic spectral bands. Some surface features are recognizable and have been mapped with the support of the geometric information available for JIRAM data. Spectral pixels acquired in parallel with the M image have been used to retrieve temperature.

[3]. Juno is a spinning spacecraft (2 rpm), which imposes challenging pointing and timing capabilities requirements to the onboard imaging payloads. Moreover, the propulsion at launch has been integrated planning a swing by of the Earth-Moon system as a gravity assist to increase the spacecraft's speed relative to the Sun. During that flyby the payload instruments were able to work

and check their capabilities. However, being JIRAM passively cooled, it was unable to observe the Earth. In fact, passed the Moon and moving towards the Earth, the cooling radiator was facing directly the illuminated face of our planet. In that condition the high Earth brightness combined with the proximity of the Sun induced instrument's temperatures well above its operative temperature.

[4]. JIRAM operates over a limited range of infrared wavelengths, 2–5 μm, and it is essentially composed of two channels, a slit spectrometer and an imager, sharing the same telescope, a despinning mirror and the internal calibration unit. The spectrometer's slit is co-located in the imager's FOV (Field of View) and the IR imager split in two spectral channels: L band, centered at 3.45 μm with a 290 nm bandwidth, and M band, centered at 4.78 μm with a 480 nm bandwidth (Adriani et al., 2014). To adapt the instrument to the rotating platform, a despinning flat mirror that counter-compensates the spin motion has been introduced at the telescope's entrance pupil.

[5]. Moon surface has been already remotely sensed many times in the infrared (IR) range, both from Earth-based telescopes (McCord et al., 1981; Pieters, 1993), and lunar orbiters like Clementine, Chandraayan-1's Moon Mineralogy Mapper, SELENE/MI, SP and Lunar Reconnaissance Orbiter (Tompkins and Pieters, 1999; Matsunaga et al., 2008; Ohtake et al., 2009; Pieters et al., 2009; Chin et al., 2007), and during Galileo (NIMS), Cassini (VIMS) and Rosetta (VIRTIS-M) mission's flybys (Pieters et al., v 1993; McCord et al., 2004; Filacchione, 2006). However many of these measurements have been carried out in a wavelength range shorter than 2.5 μm (NIR) or longer than 6.0 μm (TIR), outside the JIRAM's spectral working range. The main purpose of our analysis consists in verifying the on-ground radiometric calibration and, if necessary, tuning the response function of the instrument (Pieters, 1999), thus here we present some results derived from data management, taking advantage of this opportunity to check some retrieval procedures, already applied in different cases, and to optimize some image processing techniques in

view of the Jupiter encounter. In particular, JIRAM can retrieve the Moon surface temperatures and its results are compared with the LRO/Diviner equatorial temperature map (Vasavada et al., 2012.

[6]. Section 2 describes how JIRAM acquired the Moon observations, Section 3 concerns the data management and image processing techniques used to pass from the instrument's spectral images to the targeted region map and Section 4 deals with the Bayesian method used to retrieve surface temperature from each spectral pixel measured by the JIRAM spectrometer. Finally in the Section 5 a preliminary evaluation of our results, compared to current knowledge on this topic, is traced along with the future tasks pointed out from this first working test.

## 2. Observations

[7]. During Juno's Earth fly-by, on October 9, 2013, science instruments were switched on for their status and responsivity checking. While the spacecraft was moving towards the Earth, JIRAM was active, targeting the Moon, since 12:54 up to 14:05 UTC. Throughout this time period the spacecraft moved along its counterclockwise Sun orbit passing between Earth (on the left) and Moon (on the right). In the pass geometrical configuration, the Sun was approximately in the opposite direction of the spacecraft motion versus and the Moon, at the Juno's closest approach, was divided in two halves by the terminator. In this configuration JIRAM's telescope swept the body that appeared as entering in the image plane from the left and crossing it towards the right side. In Figure 1, a sequence of four successive shots of the whole acquisition is sketched. Figure 1 outlines the JIRAM field of view (FOV), where the rectangle resumes the imager FOV projected on the imaginary plane containing the Moon. The total imager FOV is composed by halves (upper and lower in the figure) sensitive to two different spectral ranges: the astronomical bands L and M, devoted respectively to auroral and to thermal observations. The spectrometer slit is optically superimposed to the M-band imager in the position shown in the figure. Further details on the instrument working principles can be found in Adriani et al. (2014). Finally, the Moon sweeping

97 occurred in three consecutive steps: L-band imager (a), spectrometer (b,c) and M-band imager (d),
98 the boresights respectively pointing to the center of the Moon in this order.

99 [8]. 132 images both for science and calibrations in L and M bands, together with an equivalent
100 amount of spectral measurements, have been produced in this 45-minutes of acquisition. Among
101 those ones targeting the Moon two images have been chosen for a preliminary analysis. There is not
102 any particular reason in the choice as in the short period of observations the sounded region at the
103 terminator practically did not experience variations. The images in L and M bands chosen for the
104 processing are reported in Figure 2; a couple of the associated spectra, taken as examples between
105 the shadow and the saturated region, are shown in Figure 3.

106

107 **3. Image Processing and Mapping**

108

109 [9]. Basic operations as flat field correction, dark current and background subtraction from the
110 signal are already included in the standard pipeline. This section deals with the techniques used to
111 improve the image visualization for a better identification of the target's surface structures, and with
112 georeferentiation of each pixel of the images (Hueso et al., 2010).

113 [10]. The FOV of the two images in Figs 2a and 2b is characterized by a large sky background
114 area while the Moon shows a wide dynamic range: the signal in fact is varying from noise to
115 saturated values, due to the Sun illumination path, orthogonal to the instrument-target direction.
116 Thus, both the observations have been spatially resized to a region useful for the visualization and
117 corrected for the pixel brightness (hereafter mFOV). The mFOV are rectangles, different in size for
118 L and M bands, created to encompass and show the unsaturated part of the Moon. Figure 4 shows
119 the radiance collected along the Moon's equator. The mFOV rectangles have been built using the

120 data from the useful regions of the radiance profiles. The images are also affected by a
121 inhomogeneous intensity distribution along the samples – *striped look* – and by a very low contrast,
122 due to a combination of high illumination angle and low intensity on the pixels, not sufficient to
123 reveal the surface structures. Moreover we expect a large deformation of the sounded landscape,
124 because of the Moon surface curvature included in the area covered by the mFOV. Thus a
125 combination of processing steps has been applied to correct the resized spectral images in L and M
126 band. As first step the low contrast has been enhanced working on the horizontal and vertical light
127 curves, subtracting polynomial best fits of proper degree from the along-track intensity mean
128 values; then a *destriping* algorithm (Adriani et al., 2007) has been applied. The *striped look* of the
129 images is an intrinsic and systematic behavior determined by the electrical coupling of the micro-
130 electronics elements inside the sensor matrix that creates a discontinuity between adjacent sample
131 rows of the matrix (see first and second panels from left of Figure 5). Geometric information for the
132 Moon images have been computed through the support of the SPICE standard system (Acton, 1996)
133 by using spacecraft's trajectory and attitude kernels and JIRAM scanning mirror telemetry, and
134 used to geo-reference the mFOV regions, with reference to the Moon datum (Smith, 1997). Figure
135 5a and 5b show the aforementioned image elaboration process in four steps, respectively for L-band
136 and M-band images. The contrast enhancement and noise reduction reveal in both cases the same
137 topographic design, in positive (5a) and negative (5b) look, in line with the spectral properties of
138 reflectivity and thermal emissivity of the sounded regions.

139 [11]. The area imaged by JIRAM has been identified as that encompassing the Crisium,
140 Tranquillitatis and Fecunditatis Maria. However, for a definitive attribution of the visualized surface
141 structures, a layer stacking with another geo-referenced image from a different instrument has been
142 carried out. Layer stacking module by ENVI builds a new multiband file from geo-referenced
143 images of various pixel sizes, extents, and projections. The input bands are re-sampled and re-
144 projected to a common user-selected output projection and pixel size. The output file encompasses

only the data extent where all of the files overlap. Among all the observations of the near-Earth side of the Moon, an equi-rectangular projection in JPEG2000 format from the UV/VIS camera aboard the lunar orbiter Clementine (ftp://pdsimage2.wr.usgs.gov/pub/pigpen/moon/clementine/), publicly accessible on the network, has been chosen how reference band for the stacking. In Figure 6 the stacking output in a color composite model RedGreenBlue (RGB) is reported, where the Clementine camera band is the R, and the JIRAM's geo-referenced L and M bands are the G and the B respectively. Figure 6 shows that the inferred surface structures have been correctly identified. The Crisium and Fecunditatis maria dark areas, highly emitting in M band but absorbing in the VIS (camera) and NIR (L band), are shown in blue while the ridges separating those maria, reflecting in the VIS and NIR but cold and dark in the thermal range (M band), are rendered in yellow or orange (R+G in different proportions).

## 4. Thermal Emission

[12]. In order to verify the pre-flight determined JIRAM spectral calibration, the spectrometer measurements have been used to retrieve the Moon surface temperature for a comparative test with those of LRO/Diviner (Vasavada et al., 2012). We used a Bayesian approach to nonlinear inversion that already proved to be successful for Rosetta/VIRTIS data of asteroid Lutetia and comet 67P/Churyumov-Gerasimenko (Coradini et al., 2011; Keihm et al., 2012; Capaccioni et al., 2015) and for the entire set of infrared data acquired by the Dawn/VIR spectrometer at Vesta (Tosi et al., 2014). The assumptions of the Bayesian algorithm here used are described in the Appendix of Tosi et al. (2014). The most important difference is in the spectral range 3.0-4.2 μm used for the Moon, in place of the 4.5-5.0 μm one used for Vesta. This choice depends both on the opportunity to avoid the last part of the JIRAM's range 4.8-5.0 μm, which still presents calibration issues, and on the

need to sample a larger portion of the diurnal temperature profile across the Moon where saturation occurs in the 4.2-5.0 μm range. Below we briefly summarize the main points of the procedure:

- A synthetic radiance spectrum is computed by summing the reflected solar and the thermally emitted spectra, with emissivity and temperature defined by their respective first guesses: the emissivity is initially considered equal to 0.95 across the range used for the retrieval (3.0-4.2 μm in this case), while the temperature is initially assumed equal to the average brightness temperature in a spectral region where the thermal emission dominates the observed spectral radiance.

- Surface spectral reflectance is modeled by the Lommel-Seeliger photometric function, which turns out to be optimal for Moon data. No phase function is applied and no distinction is made between lunar maria and highlands.

- Spectral reflectance and spectral emissivity are related by Kirchhoff's law: $r = 1 - \varepsilon$. This is a reasonable assumption as long as we consider small electrical penetration depths like those typically sounded by IR spectrometers (a few microns to several tens of microns).

- A best fit with respect to the radiance spectrum measured by JIRAM in the same range is sought. Surface temperature and spectral emissivity, i.e. the two unknown quantities, are free to float within a given range, a priori defined, and within the in-flight instrumental noise, until convergence around stable values is achieved. However, the parameter that accounts for the spectral emissivity cannot be considered as pure emissivity as the interval of wavelength that has been chosen for the temperature retrieval is in a range where the contribution of the Sun cannot be neglected.

- Formal errors on the unknown quantities, related to random variations of the signal, are also a standard output of the Bayesian algorithm: each value of retrieved surface temperature can be associated to a formal error.

193

194 [13]. The procedure for the surface temperature retrieval has been applied to the JIRAM spectra
195 from the acquisition showed in Figure 2b. In Figure 3 two examples of non-saturated spectra with
196 their respective best-fit simulation are shown. In Figure 7 the temperature and its formal error
197 retrieval results are reported as a function of the spatial coordinate across the spectrometer's slit.
198 From left to right (i.e. with the increasing sample index), the surface temperatures rapidly increase
199 and reach the maximum values when the target is in the slit field. In the saturation region, no
200 reliable retrieval can be performed. We note that the temperatures are still relatively high outside
201 the target. This is due to the effect of a non-negligible level of straylight due to the high values of
202 the exposure time that induced signal saturation in part of the images and the spectra. That "ghost"
203 had influence on the real lower sensitivity limit of the calculated temperatures that can be set around
204 180 K for this specific observation. This inference is supported by the trend of the uncertainties
205 associated with the retrieved temperature values: formal errors increase with decreasing
206 temperature, being very low for the highest signal level and vice versa relatively high for the signal
207 low levels. By putting in relationships the temperature with the illumination angle (solar incidence
208 and emission) values of, it can be seen that small errors are associated with the low values of the
209 solar incidence angle, as it is common for the airless bodies.

210 [14]. Ultimately, we deem reliable temperature range of 180-390 K being because affected by
211 relatively small uncertainties (<5 K) a temperature range of 180-390 K. We also observe that the
212 decrease in surface temperature is very neat in correspondence of the limit between the illuminated
213 edge of the Moon and the sky background, whereas it is less steep towards the terminator, in
214 agreement with a less abrupt transition in the physical temperatures going from the dayside to the
215 nightside of the target, and consistent with the overall low thermal inertia of the Moon (50 J $m^{-2}$ $s^{-0.5}$
216 $K^{-1}$ (Spencer *et al.*, 1989)).

[15]. In Figure 8 the surface temperature measured by JIRAM as a function of the local solar time (LST) is shown along with the temperature profile retrieved by Vasavada et al. (2012). The reason for the differences (up to 20% and on average about 10%) can be found in the different range of latitude sounded by the two instruments. JIRAM observed the equatorial region in the latitude range about ±6°, whereas Diviner measurements are limited to a narrower latitudinal range ±0.2°. Moreover, the Juno spacecraft distance from the target caused the mixing of the signal coming from different geologic regions of the Moon, so the different surface properties, including thermal inertia, can explain the differences observed in comparison with Diviner results.

## 5. Discussion and Conclusions

[16]. JIRAM was not able to get any measurements in the closest approach phase of the Earth's fly-by, as the temperature of the instrument was too high to enable good observations (thermal noise inducing extremely low signal-to-noise ratio). In fact the instrument is equipped by a passive cooling system which has been designed to operate around Jupiter, namely at a much larger distance from the Sun than the Earth. The observations of the Moon, that took place a few hours before the Earth's closest encounter, were performed at relatively high instrumental temperature (detectors worked in the range 101-103 K), but that was a unique opportunity to operate JIRAM in science mode prior to the arrival at Jupiter. Unfortunately an underestimation of the instrument sensitivity entailed an overestimation in the exposure times definition, that resulted in partial saturated images and spectra. However it has been a good test for its future use at Jupiter.

239 [17]. Since Juno is a spinning spacecraft, there was the need to verify the ability of JIRAM to
240 operate. All of the previous image-spectrometers, from which JIRAM was derived, had been
241 designed to operate on not spinning spacecrafts. Then the Moon fly-by has been used to evaluate
242 the JIRAM ability of properly pointing the target even if dedicated pointing calibrations are planned
243 to be done right after the Jupiter Orbit Insertion.

244 [18]. In this occasion JIRAM has demonstrated its ability in retrieving the surface temperatures of
245 an airless body. Temperatures obtained in this Moon fly-by are generally in agreement with the
246 expected and previously observed temperatures. These findings will be very useful in view of the
247 planned science at Jupiter.

248 [19]. The JIRAM spectral calibration has been also positively tested in the 2.0-3.0 μm spectral
249 region, comparing its Moon observation with those by Chandrayaan-1 Moon Mineralogy Mapper
250 (M3) (Pieters et al., 2009), whose dataset is publicly accessible on the web
251 (http://ode.rsl.wustl.edu/moon/index.aspx). The two instruments, though conceptually similar,
252 present remarkable differences both in spectral and spatial resolution. However, a proper data
253 reduction, based on the experimented pipeline reported by McCord et al. (1981), among the others,
254 has been carried out to reduce the M3 viewing geometries to the JIRAM's ones. For that purpose
255 we used the photometric function by Hicks et al. (2011), calculated on the M3 measurements. In
256 Figure 9 the comparison between one of the JIRAM spectral pixels (red) and the M3 measurement
257 (black), after the M3 data reduction to the JIRAM's conditions of observation, is shown. The M3
258 spectrum results from a spatial average on the region in common with the JIRAM's footprint.
259 Unfortunately the JIRAM's pixel footprint is always more extended in longitude than the
260 corresponding M3 tracks on the Moon surface. This situation is illustrated in the two pictures at the
261 right side of Figure 9, where the complete JIRAM footprint is reported on the Clementine NIR
262 camera mosaic of the region (top); it appears quite twice in longitude than that on the M3

corresponding region (bottom). The incomplete overlapping between the two footprints can explain the little difference in the radiance spectral values of the two instruments.

[20]. The Moon activity will be also used to tune the Instrument Transfer Function (ITF) to increase the reliabily of calibrated spectral measurements at Jupiter. The ITF used here is the one determined from the on-ground calibration measurements. This ITF presents two spectral anomalies between 4.2 and 4.4 μm - due to a residual presence of $CO_2$ in the in the calibration facility environment - and between 4.8 and 5.0 μm - due to the non-optimal functioning of the calibration set up in that range of wavelengths. Now the JIRAM data acquired at Moon give us the opportunity to correct the spectro-radiometric calibration before the scheduled observations at Jupiter. The ITF review is now in progress.

## Acknowledgment

This work was supported by the Italian Space Agency under the ASI-INAF contracts n. I/010/10/0 and n. 2014-050-R.0. JIRAM was developed under the leadership of INAF, Italy's National Institute for Astrophysics, Rome. The instrument was built by SELEX-Galileo, Campi Bisenzio (Fi), Italy.

## References

Acton, C.H., 1996, *1996, Planet. Space. Sci.*, **44**, 65.

Adriani A., M. L. Moriconi, G. Filacchione, et al., 2007, *Mem. S.A.It. Suppl.*, **11**.

284 Adriani A., G. Filacchione, T. Di Iorio, et al., 2014, Space Science Reviews, DOI 10.1007/s11214-
285 014-0094-y.

286 Bolton S., 2012, *The Juno Mission*, European Planetary Science Congress, Madrid, Spain

287 Brown, R. H., K. H. Baines, G. Bellucci, et al., 2004, *Space Science Reviews*, **115**, 111.

288 Capaccioni F., A. Coradini, G. Filacchione, et al., 2015, *Science*, **347** (6220), doi:
289 10.1126/science.aaa0628.

290 Chin G., S. Brylow, M. Foote, et al., 2007, *Space Science Reviews*, **129**, 391.

291 Coradini A., F. Capaccioni, P. Drossart, et al., 2007, *Space Science Reviews*, **128**, 529.

292 Coradini, A., F. Capaccioni, S. Erard, et al., 2011, *Science*, **334** (6055), 492.

293 De Sanctis, M.C., A. Coradini, E. Ammannito, et al., 2011, *Space Science Reviews*, **163**, 329.

294 Filacchione G., 2006, Ph. D. Thesis, Università degli Studi di Napoli Federico II.

295 Hicks M.D., B.J. Buratti, J. Nettles, et al., 2011, JGR, 116, doi:10.1029/2010JE003733.

296 Keihm, S., F. Tosi, L. Kamp et al., 2012, *Icarus*, **221**, 395.

297 Matsunaga T., M. Ohtake, J. Haruyama, et al., 2008, *GRL*, **35**, doi: 10.1029/2008GL035868.

298 McCord T.B., R.N. Clark, B.R. Hawke, et al., 1981, *JGR*, **86**, 10883.

299 McCord T.B., A. Coradini, C.A. Hibbitts, et al., 2004 , *Icarus*, **172**, 104.

300 Ohtake M., T. Matsunaga, Y. Yokota, et al., 2010, *Space Sci Rev*, **154**, 57.

301 Piccioni, G, P. Drossart, E. Suetta, et al., 2007, ESA Publications, SP-1295.

302 Pieters, C.M.: 1993, in: Remote Geochemical Analysis: Elemental and Mineralogical Composition,
303 C. Pieters and P. Englert (eds), *Compositional diversity and stratigraphy of the Lunar crust derived*
304 *from reflectance spectroscopy*, Cambridge University Press, Cambridge.

305 Pieters C.M., J.W. Head, J .M. Sunshine, et al., 1993, *JGR-E*, **98** (17), 127.

306 Pieters, C.M., 1999, http://www.lpi.usra.edu/meetings/moon99/pdf/8025.pdf.

307 Pieters C.M., J. Boardman, B. Buratti, et al, 2009, *Current Science*, **96**, 500.

308 Rodgers, C.D.: 2000, *Inverse Methods for Atmospheric Sounding: Theory and Practice*, World
309 Scientific Publishing Co., Singapore.

310 Smith J.R.: 1997, *Introduction to Geodesy: The History and Concepts of Modern Geodesy*, John
311 Wiley & Sons, New York, NY.

312 Spencer J. R., Lebofsky, L. A., Sykes, M. V., 1989, *Icarus*, **78**, 337.

313 Tompkins S. and C. Pieters, 1999, *Meteoritics & Planetary Science*, **34**, 2541

314 Tosi F. et al., 2014, *Icarus*, **240**, 36

315 Vasavada A.R., J.L. Bandfield, B.T. Greenhagen, P.O. et al., 2012, *JGR*, **117**, E00H18.

316

317

318 **Figure captions**

319 **Figure 1**. The Moon pass thought the JIRAM FOV with different pointing: a) Moon centered on the
320 L-band imager middle line, b) to c) spectrometer slit pointing the center of the Moon which swept
321 the all slit length, and d) Moon centered on the M-band imager middle line. The white line indicates

322 the image plane field of view (L-band and M-band together), the red rectangle sketches the spectral
323 plane (here rotated in the same plane of the image one for a better visualization) and the yellow line
324 is the position of the spectrometer slit optically superimposed to the M-band imager.

325 **Figure 2**. Panel (a): Moon real image centered on the L-band imager middle line. Panel (b): Moon
326 real image centered on the spectrometer slit and contemporary imaged by the M-band imager.

327 **Figure 3**. Spectra from pixel 130 1nd 140 taken between the shadow and the saturated region. The
328 spectra correspond to the image in Figure 2b. The red line is the simulated best-fit spectrum.

329 **Figure 4**. Radiance measured along the Moon equator on IMAGER M-band. The "useful region" of
330 the image selected, shown in Figure 5 and used to build the chromatic composition of Figure 6.

331 **Figure 5**. Elaboration processes of the moon images from IMAGER L-band (a) and M-band (b).
332 Transformation processes in three steps: re-equilibration of the illumination, image de-striping, and
333 geo-referencing/Mercatore projection.

334 **Figure 6**. Color composite RGB image: the Clementine camera image in the red color, the
335 JIRAM's geo-referenced L-band in green and JIRAM's geo-referenced M-band in blue.

336 **Figure 7**. Top: Temperatures retrieved by the JIRAM spectrometer as a function of the slit sample.
337 Bottom: Formal error (standard deviation) on the retrieved temperatures.

338 **Figure 8**. Temperatures retrieved by the JIRAM spectrometer as a function of the local solar time
339 (black line). A comparison with LRO/Diviner results by Vasavada et al. (2012) is also shown (red
340 line).

341 **Figure 9**. Comparison between M3 (black curve) and JIRAM spectra (red curve) in the spectral
342 range 2-3 μm. The grey area on the plot represents the M3 spectrum plus or minus the standard
343 deviation obtained by the averaging all the spectra overlapping the JIRAM area. The two pictures

on the right are Clementine's image (up) and M3's image (low). The red polygons represent the JIRAM pixel. Clementine is used as reference to show that the area covered by M3 is roughly about a half of the JIRAM pixel.

## Figures

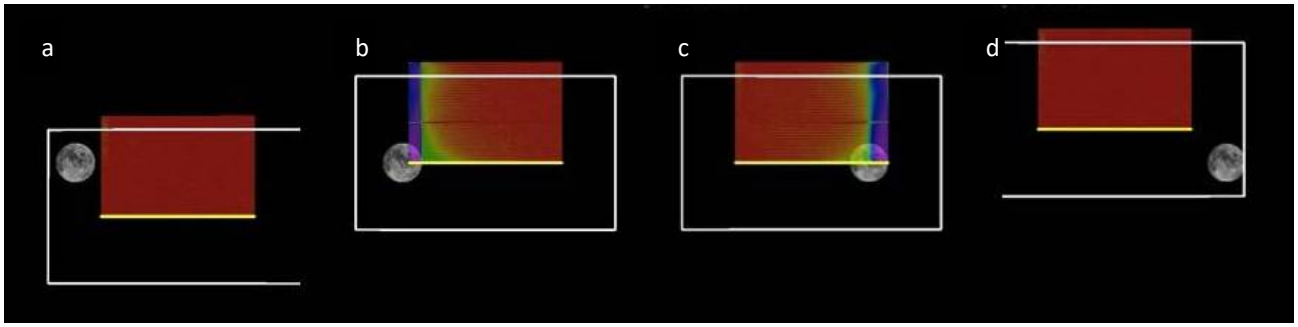


Figure 1

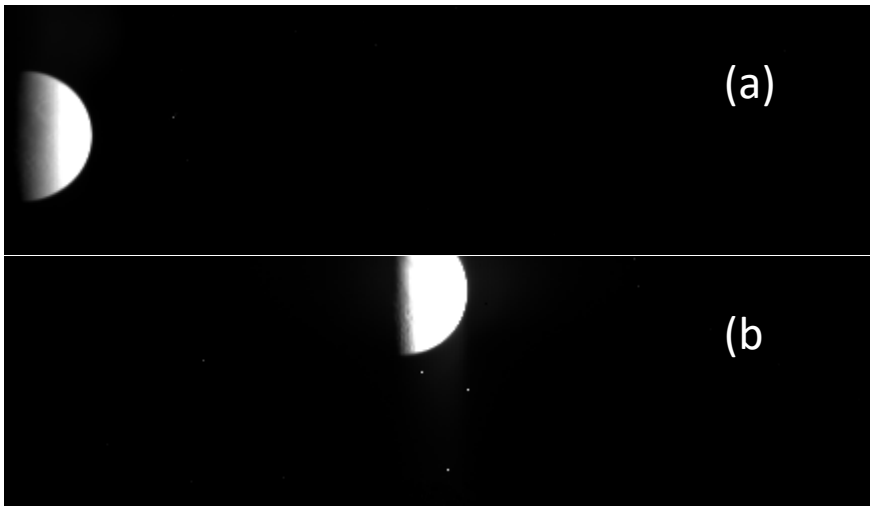


Figure 2

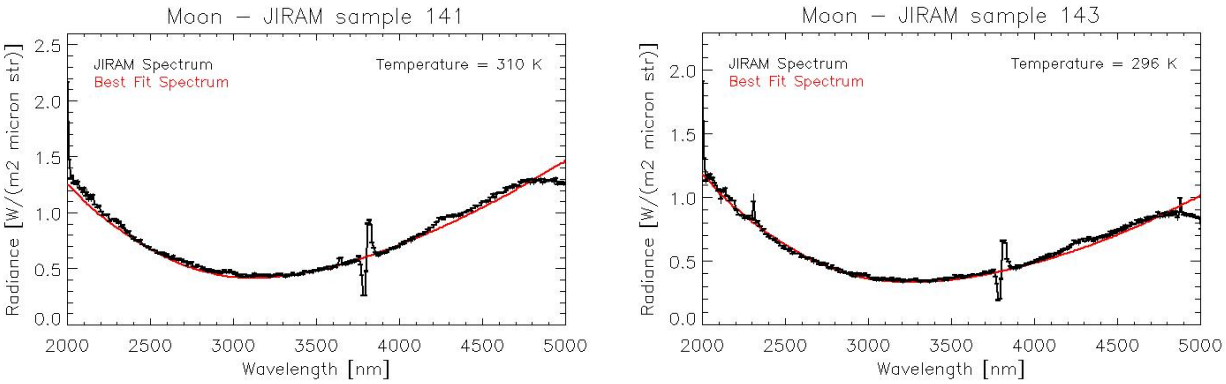


Figure 3

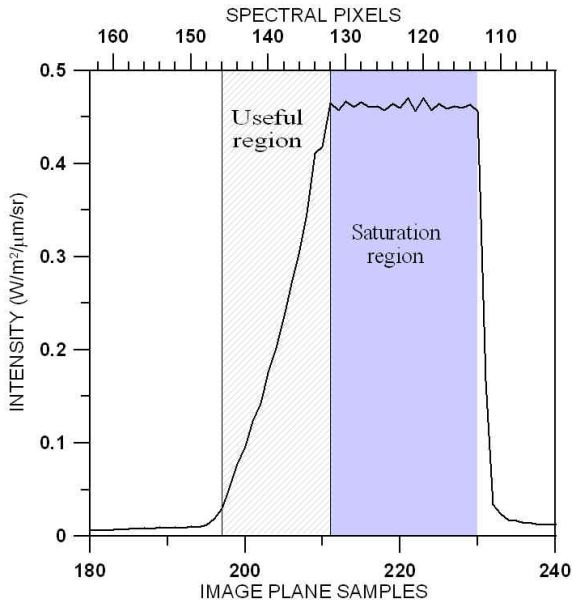


Figure 4

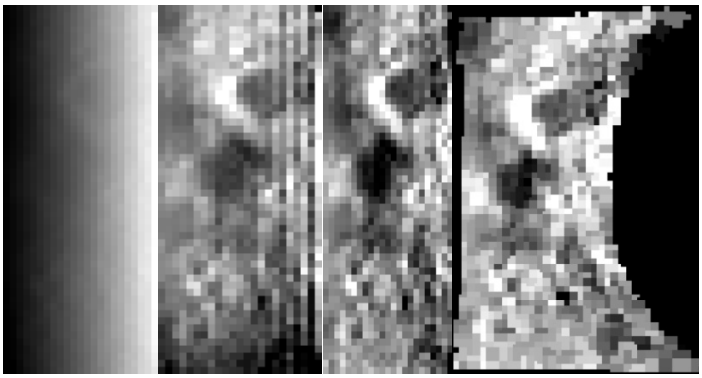

Figure 5a

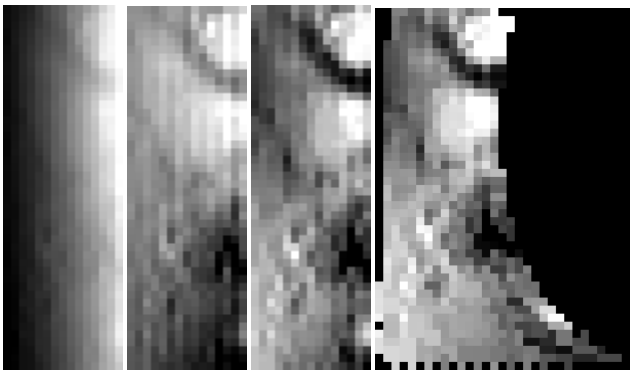

Figure 5b

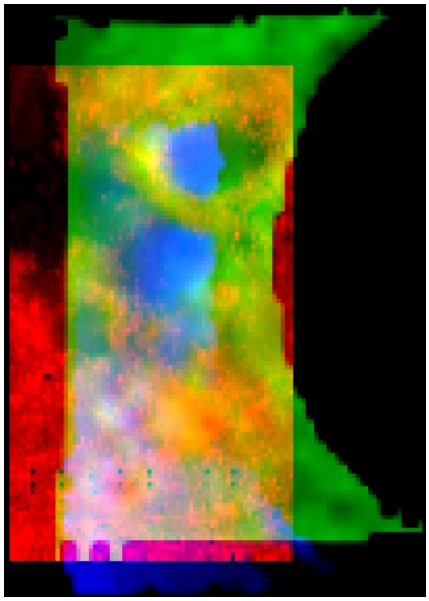

**Figure 6**

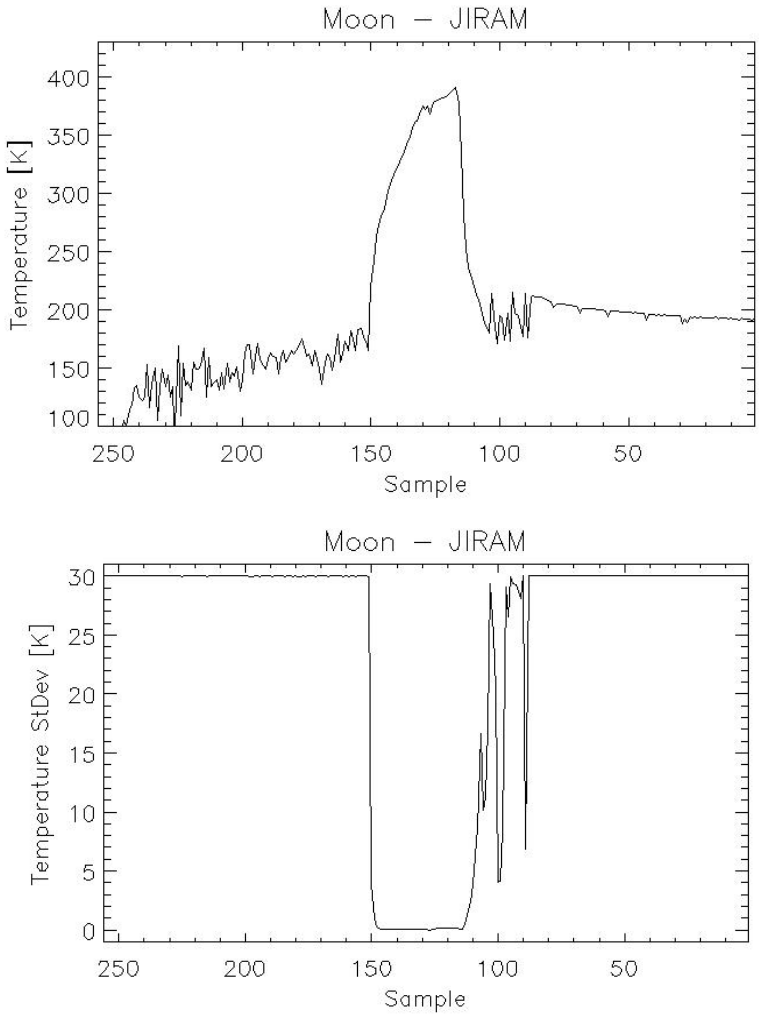


388

389

390

Figure 7

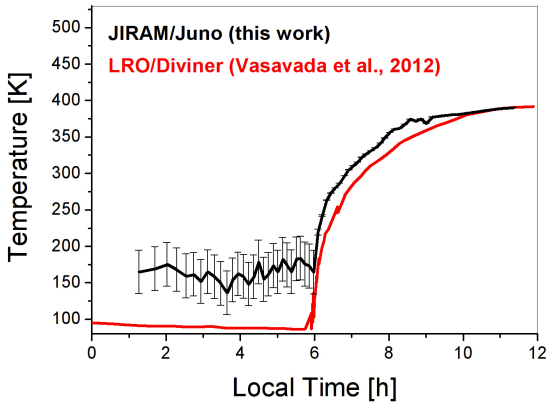


391

392 Figure 8

393

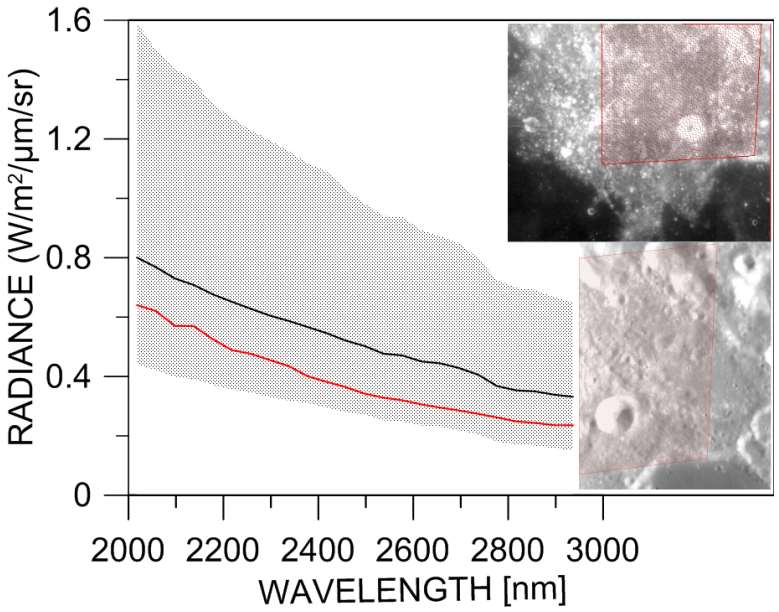
1.6
1.2
0.8
0.4
0
RADIANCE (W/m²/µm/sr)
2000
2200
2400
2600
2800
3000
WAVELENGTH [nm]

Figure 9.